


## Research Article

# The depletion of star-forming gas by AGN activity in radio sources

S. J. Curran 

School of Chemical and Physical Sciences, Victoria University of Wellington, Wellington, New Zealand

### Abstract

Cold, neutral interstellar gas, the reservoir for star formation, is traced through the absorption of the 21-cm continuum radiation by neutral hydrogen (H I). Although detected in one hundred cases in the host galaxies of distant radio sources, only recently have column densities approaching the maximum value observed in Lyman- $\alpha$  absorption systems ( $N_{\text{HI}} \sim 10^{22} \text{ cm}^{-2}$ ) been found. Here, we explore the implications these have for the hypothesis that the detection rate of H I absorption is dominated by photo-ionisation from the active galactic nucleus (AGN). We find, with the addition all of the current searches for H I absorption at  $z \geq 0.1$ , a strong correlation between the H I absorption strength and the ionising photon rate, with the maximum value at which H I is detected remaining close to the theoretical value in which all of the neutral gas would be ionised in a large spiral galaxy ( $Q_{\text{HI}} = 2.9 \times 10^{56} \text{ ionising photons s}^{-1}$ ). We also rule out other effects (excitation by the radio continuum and changing gas properties) as the dominant cause for the decrease in the detection rate with redshift. Furthermore, from the maximum theoretical column density, we find that the five high column density systems have spin temperatures close to those of the Milky Way ( $T_{\text{spin}} \lesssim 300 \text{ K}$ ), whereas, from our model of a gaseous galactic disc, the H I detection at  $Q_{\text{HI}} = 2.9 \times 10^{56} \text{ s}^{-1}$  yields  $T_{\text{spin}} \sim 10\,000 \text{ K}$ , consistent with the gas being highly ionised.

**Keywords:** Galaxies: active; quasars: absorption lines; radio lines: galaxies; ultraviolet: galaxies; galaxies: fundamental parameters; galaxies: ISM

(Received 15 December 2023; accepted 29 December 2023)

### 1. Introduction

Since the first high redshift ( $z \gtrsim 3$ ) survey for cold neutral (star-forming) gas, via the absorption of the 21-cm transition of neutral hydrogen in the host galaxies of distant radio sources, it has been posited that the dearth of detections is due to the selection of ultraviolet (UV) luminous sources. In these objects, the UV radiation from the active galactic nucleus (AGN) is sufficient to ionise the gas to below the detection limits of large radio telescopes (Curran et al. 2008b). While a steady decrease with redshift, and hence UV luminosity, may be expected, an abrupt cut-off in the detection of H I above  $L_{\text{UV}} \sim 10^{23} \text{ W Hz}^{-1}$  (ionising photon rates of  $Q_{\text{HI}} \gtrsim 10^{56} \text{ s}^{-1}$ ) is apparent. Curran & Whiting (2012) showed that such a critical luminosity would arise from an exponential gas distribution, with the observed value being close that required to ionise all of the gas in the Milky Way, that is, a large spiral.

Since then, this observational result has been confirmed, not only over specific ‘homogeneous’ subsets of sources (compact, extended, flat spectrum, etc., Curran et al. 2013b, 2016; Aditya, Kanekar, & Kurapati 2016; Aditya & Kanekar 2018a; Grasha et al. 2019; Murthy et al. 2021, 2022), but also unbiased samples, limited only by flux (Curran et al. 2011, 2013a, 2017a,b, 2019; Allison et al. 2012; Geréb et al. 2015). The complete ionisation of the gas within the host galaxies of these objects would prevent star formation within them and is strongly indicative of a selection effect, where the traditional need for a reliable optical redshift, to which

to tune the radio band receiver, causes a bias towards the most UV luminous sources (Curran et al. 2008b). This suggests a population of undetected gas-rich galaxies in the distant Universe, too faint to be detected via optical spectroscopy.

There is, however, still some debate over this interpretation: Curran et al. (2008b) also noted that all of the sources above the critical UV luminosity were type 1 objects (quasars), suggesting that the gas could be undetected due to the obscuring circum-nuclear torus, invoked by unified schemes of AGN (Osterbrock 1978; Antonucci & Miller 1985; Miller & Goodrich 1987), not intercepting our sight-line to the AGN. However, below the critical UV luminosity the detection rate was similar to that in type-2 objects (galaxies), suggesting that the bulk of the absorption occurs in the large-scale galactic disk, which is randomly orientated to the pc-scale torus (Curran & Whiting 2010). Furthermore, rather than photo-ionisation from the AGN being the dominant cause of the decrease in detection rate with redshift, Aditya & Kanekar (2018a,b), Aditya et al. (2024) propose excitation of the hydrogen by 1.4 GHz photons (Purcell & Field 1956; Field 1959) or some other (unspecified) evolutionary effect. While the former has been ruled out (Curran et al. 2008b, 2019, see also Section 3.1.3), the latter effects would have to apply across the whole sample, irrespective of source classification in order to usurp the ionisation hypothesis.

Most recently, there have been five detections of H I absorption (Chowdhury, Kanekar, & Chengalur 2020; Murthy et al. 2021; Su et al. 2022; Aditya et al. 2024), where the column density would exceed the theoretical limit of  $N_{\text{HI}} \sim 10^{22} \text{ cm}^{-2}$  (Schaye 2001), for moderate spin temperatures. In this paper, we reassess the ionisation hypothesis in light of these and the vastly increased sample of published H I searches.

Email: Stephen.Curran@vuw.ac.nz

**Cite this article:** Curran SJ. (2024) The depletion of star-forming gas by AGN activity in radio sources. *Publications of the Astronomical Society of Australia* 41, e007, 1–8. <https://doi.org/10.1017/pasa.2024.1>

## 2. Analysis

### 2.1. The data

Adding the recent searches, comprising 441 objects (Chowdhury et al. 2020; Murthy et al. 2021, 2022; Mahony et al. 2022; Su et al. 2022; Aditya et al. 2024; Deka et al. 2024), to those compiled in Curran et al. (2019) there are now 924  $z \geq 0.1$  sources in the literature which have been searched for associated H I 21-cm absorption. These are made up of 100 detections and 824 non-detections.

### 2.2. Photometry and fitting

To obtain the ionising photon rate for each of the 924 sources, their photometry were scraped from the *NASA/IPAC Extragalactic Database* (NED), the *Wide-Field Infrared Survey Explorer* (WISE, Wright et al. 2010), *Two Micron All Sky Survey* (2MASS, Skrutskie et al. 2006), and the *Galaxy Evolution Explorer* (GALEX, data release GR6/7)<sup>a</sup> databases. After shifting the data back into the source's rest-frame, each flux density measurement,  $S_\nu$ , was then converted to a specific luminosity, via  $L_\nu = 4\pi D_L^2 S_\nu / (z + 1)$ , where  $D_L$  is the luminosity distance to the source (see Fig. 1).<sup>b</sup> To obtain the ionising photon rate, we use (Osterbrock 1989):

$$Q_{\text{HI}} \equiv \int_{\nu_{\text{ion}}}^{\infty} \frac{L_\nu}{h\nu} d\nu, \quad (1)$$

where  $\nu$  is the frequency (with  $\nu_{\text{ion}} = 3.29 \times 10^{15}$  Hz for H I) and  $h$  the Planck constant. Fitting the rest-frame UV data with a power-law fit,  $L_\nu \propto \nu^\alpha$ , gives

$$\log_{10} L_\nu = \alpha \log_{10} \nu + C, \quad (2)$$

where  $C$  is the log-space intercept and  $\alpha$  the gradient (the spectral index). Integrating this over  $\nu_{\text{ion}}$  to  $\infty$  gives the ionising photon rate as:

$$Q_{\text{HI}} = \frac{-10^C}{\alpha h} \nu_{\text{ion}}^\alpha, \quad (3)$$

shown by the shaded region in Fig. 1. In order to ensure a sufficient sample size, while not contaminating the UV with optical band data, we fit all photometry with  $\log_{10} \nu \geq 15.1$  (shown by the dotted line in the figure), which left 180 sources with sufficient UV data. Of these, 19 have been detected in H I.

### 2.3. H I absorption strength

The strength of the H I 21-cm absorption is given by the profile's velocity-integrated optical depth ( $\int \tau d\nu$ ), which is analogous to the equivalent width in optical-band spectroscopy. This is related to the total neutral hydrogen column density via

$$N_{\text{HI}} = 1.823 \times 10^{18} T_{\text{spin}} \int \tau d\nu, \quad (4)$$

where the spin temperature,  $T_{\text{spin}}$ , quantifies the excitation from the lower hyperfine level of the hydrogen atom (Purcell & Field 1956).

We do not measure the intrinsic optical depth directly, but rather the observed optical depth,  $\tau_{\text{obs}}$ , which is the ratio of the

<sup>a</sup><http://galex.stsci.edu/GR6/#mission>.

<sup>b</sup>We use  $H_0 = 67.4 \text{ km s}^{-1} \text{ Mpc}^{-1}$  and  $\Omega_m = 0.3125$  (Planck Collaboration et al. 2020) throughout the paper.

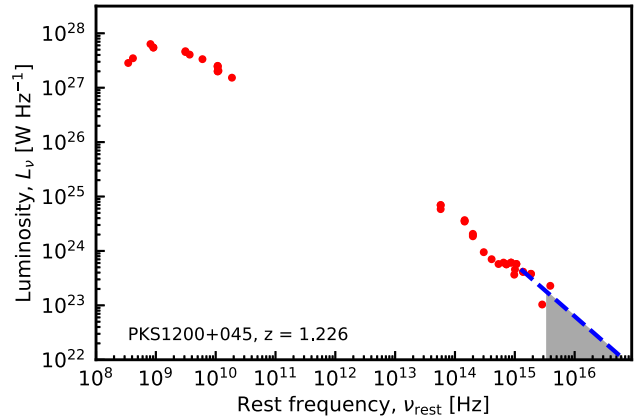


**Figure 1.** Example of the rest-frame photometry. The dotted line shows the power-law fit to the UV data and the shaded region  $\nu \geq 3.29 \times 10^{15}$  Hz over which the ionising photon rate is calculated. Here, we show PKS 1200+045, which with  $Q_{\text{HI}} = 2.9 \times 10^{56} \text{ s}^{-1}$  is the highest ionising photon rate at which H I absorption has been detected (see Section 3.3).

line depth,  $\Delta S$ , to the observed background flux,  $S_{\text{obs}}$ . The two are related via

$$\tau \equiv -\ln \left( 1 - \frac{\tau_{\text{obs}}}{f} \right) = -\ln \left( 1 - \frac{\Delta S}{f S_{\text{obs}}} \right), \quad (5)$$

where the covering factor,  $f$ , is the fraction of  $S_{\text{obs}}$  intercepted by the absorber. In the optically thin regime, where  $\tau_{\text{obs}} \lesssim 0.3$ ,  $\tau \approx \tau_{\text{obs}}/f$ , so that Equation (4) can be approximated as:

$$N_{\text{HI}} \approx 1.823 \times 10^{18} \frac{T_{\text{spin}}}{f} \int \tau_{\text{obs}} d\nu. \quad (6)$$

For the non-detections, the upper limit to the line strength is obtained via  $\tau_{\text{obs}} = 3\sigma_{\text{rms}}/S_{\text{obs}}$ , where  $\sigma_{\text{rms}}$  is the rms noise level of the spectrum. In order to place each of the limits on an equal, footing each is re-sampled to the same spectral resolution ( $\Delta\nu = 20 \text{ km s}^{-1}$ ), which is then used as the full-width at half maximum to obtain the integrated optical depth limit per channel (see Curran 2012).

Common practice is to convert the observed velocity integrated optical depth to a column density, by assuming the spin temperature (and, presumably,  $f = 1$ , e.g. Su et al. 2023). However, since we have no information on this, or the covering factor,<sup>c</sup> we define the *normalised line strength*:

$$1.823 \times 10^{18} \int \tau_{\text{obs}} d\nu, \text{ which gives } N_{\text{HI}} \left( \frac{f}{T_{\text{spin}}} \right). \quad (7)$$

Showing the distributions in Fig. 2, we see that while, in general, the non-detections have been searched sufficiently deeply to detect H I absorption, the sample of Su et al. (2022) may not have been.<sup>d</sup> In order to reduce any bias by including weaker limits, in the rest of the analysis we only consider non-detections searched to  $N_{\text{HI}} \leq 10^{19} (T_{\text{spin}}/f) \text{ cm}^{-2}$ .

<sup>c</sup>Where  $N_{\text{HI}}$  is available, either from 21-cm emission at  $z \lesssim 0.1$  or Lyman- $\alpha$  absorption (at  $z \lesssim 1.7$  with ground-based instruments),  $T_{\text{spin}}/f$  can be measured, although this varies greatly between objects: 40–300 K within the Milky Way (Strasser & Taylor 2004) and  $10 \lesssim T_{\text{spin}}/f \lesssim 10^4$  K at high redshift (Curran 2019), as well across individual objects: In near-by galaxies this is  $T_{\text{spin}}/f \approx 2000$  K within the stellar disc at galactocentric radii of  $r \lesssim 10$  kpc before peaking at  $T_{\text{spin}}/f \approx 7000$  K at  $r \approx 15$  kpc (Curran 2020), where the OB stars are concentrated (Morgan, Whitford, & Code 1953).

<sup>d</sup>Most likely due to their selection of very faint continuum sources ( $S_{\text{obs}} \lesssim 10 \text{ mJy}$ ).

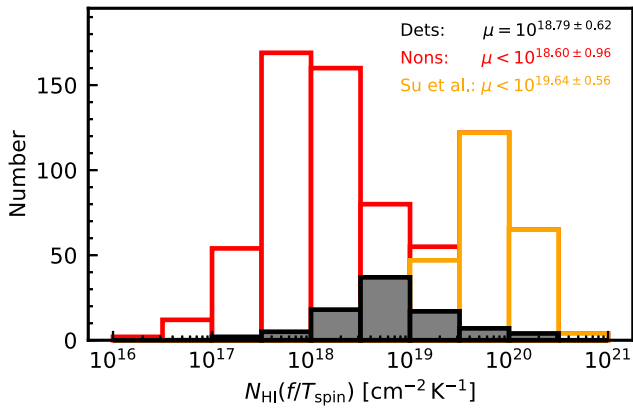


**Figure 2.** The distributions of the normalised line strengths for the detections (filled histogram) and the upper limits (unfilled), which have been separated into the upper limits of Su et al. (2022) and the rest of the sample. The legend shows the mean ( $\pm 1\sigma$ ) value of each distribution.

### 3. Results and discussion

#### 3.1. Factors affecting the detection of H I

##### 3.1.1. Source classification

In Fig. 3, we show the derived ionising photon rates versus the look-back time/redshift. At low redshifts, we can see the high detection rate reported previously (e.g. Vermeulen et al. 2003; Maccagni et al. 2017). At best, we would expect a  $\approx 50\%$  rate from the random orientation of the absorbing medium, whether this be in the obscuring torus or the large-scale galactic disk. However, it is clear that there is a sharp decrease in the detection rate with redshift, which may be caused by the preferential selection of type 1 objects (quasars), where the AGN is not obscured by the torus.

The galaxy and quasar detection rates are shown in Fig. 4. Ignoring the 50 and 100% values, which comprise only one or two objects, we see that both detection rates drop with increasing  $Q_{\text{HI}}$ . This is much steeper for galaxies, although these start from much higher values. Below the critical UV luminosity, Curran et al. (2008b) found a  $53 \pm 10\%$  detection rate for galaxies and  $33 \pm 13\%$  for quasars at  $L_{\text{UV}} \lesssim 10^{23} \text{ W Hz}^{-1}$ . The current numbers are smaller as we use the more stringent  $\log_{10} \nu \geq 15.1$ , cf.  $\log_{10} \nu \geq 14.8$ , for the UV data, as well as the ionising photon rate (by integrating the UV photometry), rather than the monochromatic luminosity, which requires more complete UV photometry. If we ignore the small number statistics,<sup>e</sup> this suggests that the orientation of the torus may play a role, but given that quasars are nevertheless detected in H I absorption, this cannot be the whole story. Note also that Murthy et al. (2022) do not detect absorption in any of their 29 targets, considered to be galaxies and therefore expected to yield several detections. However, the choice of targeting extended objects may bias towards lowering covering factors, the effect of which is suspected of reducing the observed optical depth in extended radio sources (Curran et al. 2013c).

Lastly, there is the simple explanation that quasars are generally more luminous than galaxies (e.g. Antonucci 1993) and, by scaling, have correspondingly higher ionisation rates. This is apparent

<sup>e</sup>The first three quasar bins have a total of just 4 quasars for  $Q_{\text{HI}} < 10^{54} \text{ s}^{-1}$ , 21 for  $10^{54} < Q_{\text{HI}} < 10^{56} \text{ s}^{-1}$  and 40 for  $10^{56} < Q_{\text{HI}} < 10^{58} \text{ s}^{-1}$ .

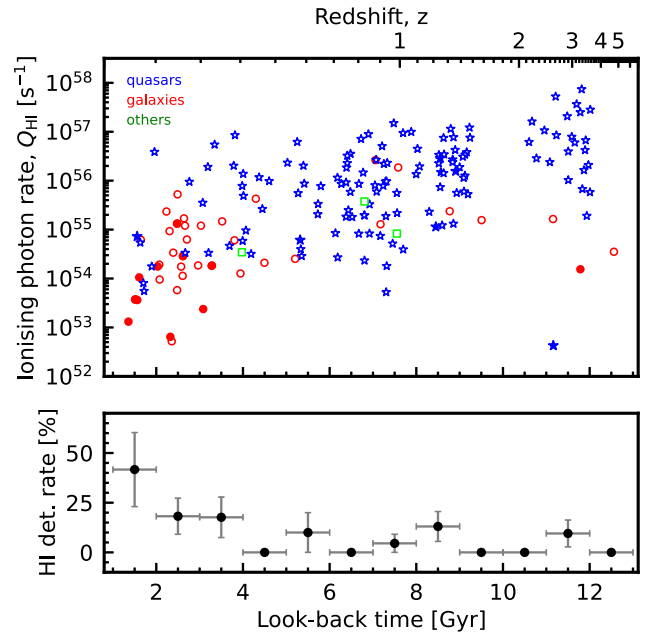


**Figure 3.** The ionising photon rate versus the look-back time. The filled symbols show the H I detections and the unfilled the non-detections, with the shapes designating the source classification: quasars – stars, galaxies – circles, other – squares. The lower panel shows the H I detection rate at various look-back times, where the error bars on the ordinate show the Poisson standard errors and abscissa the range over which these apply.

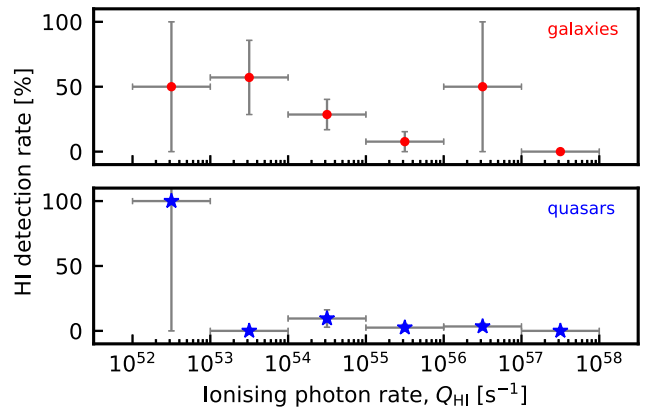


**Figure 4.** The detection rate versus the ionising photon rate for the galaxies and the quasars. The error bars are as described in Fig. 3. For the galaxies, the exact 50% detection rates are due to a single detection and non-detection in the range and the 100% detection rate for the quasars is due to only having a single object in the range. The H I detected galaxy in the  $Q_{\text{HI}} = 10^{56} - 10^{57} \text{ s}^{-1}$  bin is PKS 1200+045 (see Section 3.3).

in Fig. 5, where the UV and radio luminosities are strongly correlated [ $p(\tau) = 2.17 \times 10^{-14}$ ]. That is, the Malmquist bias towards brighter objects at high redshift, and fainter objects at low redshift, means that the brighter quasars will be more UV luminous resulting in a lower H I detection rate.

##### 3.1.2. Ionising photon rate

In Fig. 6, we show the distribution of the normalised line strengths versus the ionising photon rates for the sources which have sufficient UV photometry. For the 19 detections alone, the Kendall’s tau test gives a probability of  $p(\tau) = 0.046$  for the

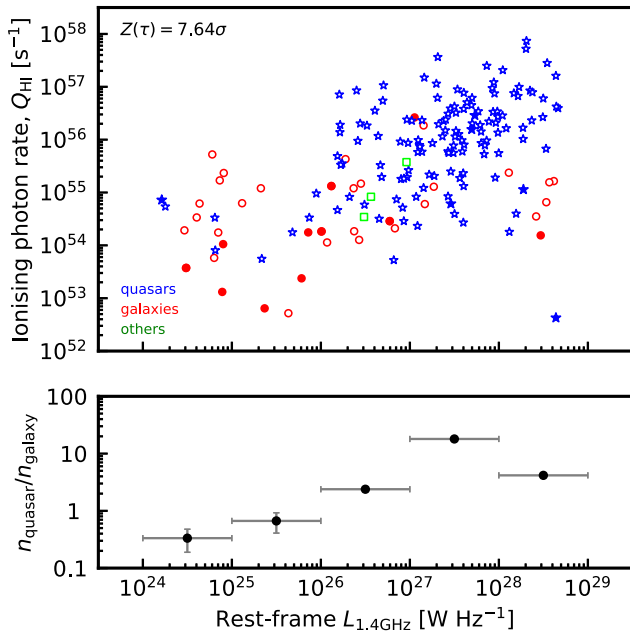


**Figure 5.** The ionising photon rate versus the 21-cm continuum luminosity. The bottom panel shows the ratio of quasars to galaxies in each  $L_{1.4\text{ GHz}}$  bin.

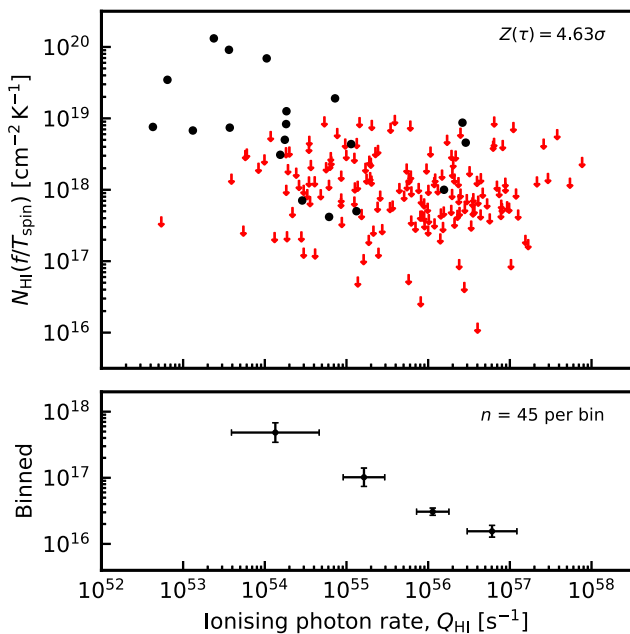


**Figure 6.** The normalised absorption strength versus the ionising photon rate. The circles show the detections and the arrows the  $3\sigma$  upper limits re-sampled to  $\Delta v = 20\text{ km s}^{-1}$ . The lower panel shows the data in equally sized bins with  $\pm 1\sigma$  error bars.

$N_{\text{HI}}/(fT_{\text{spin}}) - Q_{\text{HI}}$  anti-correlation occurring by chance. This is significant at  $1.99\sigma$ , assuming Gaussian statistics. If we include the upper limits, as censored data points, via the *Astronomy SURVival Analysis* (ASURV) package (Isobe, Feigelson, & Nelson 1986), the probability becomes  $p(\tau) = 3.66 \times 10^{-6}$  ( $4.63\sigma$ ).

Of the five absorbers with  $N_{\text{HI}} \gtrsim 10^{20} (T_{\text{spin}}/f)\text{ cm}^{-2}$ , only one has sufficient UV photometry to obtain the ionising photon rate (WISEA J145239.38+062738.2). With  $Q_{\text{HI}} = 2.4 \times 10^{53}\text{ s}^{-1}$ , this is

well below the  $Q_{\text{HI}} \sim 10^{56}\text{ s}^{-1}$  cut off. However, from the binning in Fig. 6, the anti-correlation between absorption strength and ionising photon rate is clear.<sup>f</sup> Lastly, below the maximum detected value of  $Q_{\text{HI}} = 2.9 \times 10^{56}\text{ s}^{-1}$  there are 19 detections and 124 non-detections, giving a detection rate of 13.3%. Above the maximum detected value, there are 40 non-detections and, of course, 0 detections. For  $p = 0.133$ , the binomial probability of obtaining 0 detections out of 40 at  $Q_{\text{HI}} > 2.9 \times 10^{56}\text{ s}^{-1}$  is  $3.32 \times 10^{-3}$  ( $2.94\sigma$ ).

Bear in mind that there will be significant noise in these data, due to different source sizes and morphologies (see Section 3.1.4), and the fact that a large fraction of the non-detections will simply not be orientated favourably for us to detect absorption. This would give, at best, a  $\approx 50\%$  detection rate (Section 3.1.1) and if these could be removed, leaving only the ionisation as the factor under consideration, we could see much more significant results.

### 3.1.3. Radio luminosity

As stated above, Aditya & Kanekar (2018a,b) propose the excitation of the hydrogen by 1.4 GHz photons as a factor in the decrease in detection rate with redshift, although this was ruled out by Curran et al. (2008b). Returning to this, in Fig. 7, we see that the HI absorption strength also exhibits an anti-correlation with the 21-cm continuum luminosity, although with  $p(\tau) = 0.0020$  this is considerably weaker than for the ionising photon rate. Furthermore, unlike for  $Q_{\text{HI}}$ , it is seen that the detections and non-detections occupy a very similar range of luminosities. Quantifying this, below the maximum detected value of  $L_{1.4\text{ GHz}} = 4.7 \times 10^{28}\text{ W Hz}^{-1}$  there are 85 detections and 437 non-detections, giving a detection rate of 16.3%. Above the maximum detected value, the 6 non-detections therefore give a binomial probability of 0.344 ( $0.95\sigma$ ) of the distribution arising by chance. Thus, unlike the UV luminosity, there is no evidence of a critical radio luminosity, above which HI is not detected (as previously found by Curran et al. 2008b, 2019). We also note that a correlation between the line strength and radio luminosity would be expected just from scaling with the ionising photon rate (see Fig. 5).

### 3.1.4. Other effects

Aditya & Kanekar (2018a,b) and Aditya et al. (2024) also propose other redshift evolutionary effects as the cause of the decrease in detection rate with redshift. Regarding each of these:

- *Source morphology:* It has long been known that the HI absorption strength is anti-correlated with the size of the source (Pihlström et al. 2003), which Curran et al. (2013c) suggested is a geometry effect introduced by the covering factor, and so we do expect higher detection rates in compact objects. However, given that HI is detected over a range of source sizes, and neither compact nor non-compact objects are detected above the critical UV luminosity (Curran & Whiting 2010), the ionisation argument remains the more comprehensive.
- *Gas properties:* Evolving gas properties could arise from either a changing column density or evolving spin temperature (see Sections 3.2 & 3.3). Due to the weakness of HI 21-cm emission, we do not usually have a measure of  $N_{\text{HI}}$  at  $z \lesssim 0.1$ , although, from the spectra of damped Lyman- $\alpha$  absorption systems (DLAs), there is no evidence of any

<sup>f</sup>The limits are included via the Kaplan & Meier (1958) estimator.

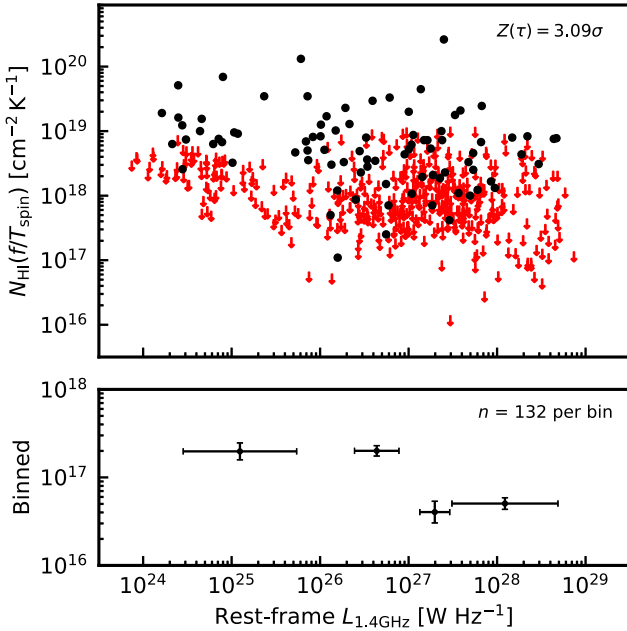


Figure 7. As Fig. 6, but for the 21-cm continuum luminosity.

evolution for intervening absorbers (Curran 2019 and references therein). Another possibility is an increase in the spin temperature of the gas (cf. the decrease in covering factor above). However, this would be expected to be a result of the high ionisation rates.

- *AGN luminosity*: Again, this would be a signature of the ionising photon rate, since we have ruled out the effect of the radio luminosity (Section 3.1.3).

Aditya & Kanekar also propose an unspecified evolutionary effect. Due to the Malmquist bias, the ionising photon rate is strongly correlated with the redshift (Fig. 3) and we can test this as above: The maximum redshift at which H I has been detected is  $z = 3.530$  (Aditya et al. 2021). Below this redshift, there are 90 detections and 711 non-detections with  $N_{\text{HI}} \leq 10^{19} (T_{\text{spin}}/f) \text{ cm}^{-2}$ , giving a detection rate of 11.2%. Thus, the binomial probability of obtaining 0 detections out of 12 at  $z > 3.530$  is  $p = 0.240$  ( $1.17\sigma$ ). That is, the detection of H I appears to be much more dependent on the photo-ionisation than the redshift, although both properties are intimately entwined.

### 3.2. High column density systems

In Galactic high latitude clouds, above column densities of  $N_{\text{HI}} \approx 4 \times 10^{20} \text{ cm}^{-2}$  (Reach, Koo, & Heiles 1994; Heithausen et al. 2001)<sup>8</sup> the H I begins to form  $\text{H}_2$ , with Schaye (2001) suggesting that this is the reason why high redshift absorbers (DLAs) are never found with column densities  $N_{\text{HI}} \gtrsim 10^{22} \text{ cm}^{-2}$ . Applying this to the current sample, Curran & Whiting (2012) used a simple exponential model of the Galactic gas distribution,  $n = n(0)e^{-r/R}$ , where  $R$  is the scale-length of the decay. Extrapolating from  $n = n_0 e^{-(r-R_\odot)/R}$ , where  $n_0 = 0.9 \text{ cm}^{-3}$ ,  $R_\odot = 8.5 \text{ kpc}$  and  $R = 3.15 \text{ kpc}$  (Kalberla & Kerp 2009) to  $r = 0$ , gave  $n(0) = 13.4 \text{ cm}^{-3}$ . The total

<sup>8</sup>This limit is also apparent in the near-by Circinus galaxy (Curran, Koribalski, & Bains 2008a).

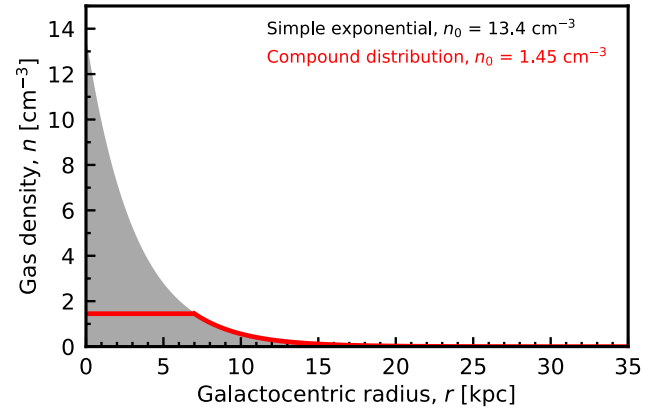


Figure 8. The gas density versus the galactocentric radius for the simple exponential (grey) and compound (red) models of the Milky Way.  $r_0$  is radius at which the break between the models occurs.

column density between the continuum source and ourselves is therefore

$$N_{\text{HI}} = \int_0^\infty n dr = n(0) \int_0^\infty e^{-r/R} dr = n(0)R$$

$= 1.3 \times 10^{23} \text{ cm}^{-2}$ , which is about an order of magnitude higher than that expected.

We therefore proceed by using a compound model, where a constant density component is added over  $0 \leq r \leq r_0$  to the exponential component (Fig. 8), giving

$$N_{\text{HI}} = \int_0^{r_0} n_0 dr + \int_{r_0}^\infty n_0 e^{-(r-R_\odot)/R} dr, \quad (8)$$

where  $n_0 = 0.9 \text{ cm}^{-3}$ ,  $R = 3.15 \text{ kpc}$ ,  $R_\odot = 8.5 \text{ kpc}$  and  $r_0 = 7 \text{ kpc}$  (Kalberla & Kerp 2009). To reduce the number of free parameters, we rewrite the formula of Kalberla & Kerp:

$$n = n_0 e^{-(r-R_\odot)/R} \text{ as } n = n_0 e^{-(r-r_0)/R},$$

where  $n = 0$  is now the gas density at  $r_0$ , e.g.  $n_0 = 1.45 \text{ cm}^{-3}$  at  $r_0 = 7 \text{ kpc}$ , cf.  $n_0 = 0.9 \text{ cm}^{-3}$  at  $R_\odot = 8.5 \text{ kpc}$  for the Milky Way (Fig. 8). Making the substitution and integrating, Equation (8) becomes

$$N_{\text{HI}} = n_0 (r_0 + R e^{-r_0/R}), \quad (9)$$

giving  $N_{\text{HI}} = 3.3 \times 10^{22} \text{ cm}^{-2}$ , which is closer to the expected limit.

Since this value is obtained through an inclined disc, we may expect it to be close to representing the theoretical limit. For the five H I absorbers with  $N_{\text{HI}} \lesssim 10^{20} (T_{\text{spin}}/f) \text{ cm}^{-2}$  the absorption is optically thick and so the approximation in Equation (6) cannot be used unless  $f = 1$ . In any case, having  $f < 1$  would have the effect of decreasing the already low spin temperatures (Table 1).

Such spin temperatures are typical of the Milky Way ( $T_{\text{spin}} \lesssim 300 \text{ K}$ , Strasser & Taylor 2004; Dickey et al. 2009), but may be atypical in sources host to a powerful AGN. As mentioned in Section 3.1.1, the ionising photon rate is only available for one of these (WISEA J145239.38+062738.2), which has  $Q_{\text{HI}} = 2.4 \times 10^{53} \text{ s}^{-1}$ . This is three orders of magnitude below the highest value where H I has been detected. Furthermore, this, and the other three high column density systems, are at redshifts  $z \ll 3$ , meaning that the optical-band observation which yielded the redshift are not close to the rest-frame UV band. This was identified as introducing a possible bias by Curran et al. (2008b), where the

**Table 1.** The five  $N_{\text{HI}} \gtrsim 10^{20}$  ( $T_{\text{spin}}/f$ )  $\text{cm}^{-2}$  absorbers (Chowdhury et al. 2020; Murthy et al. 2021; Su et al. 2022; Aditya et al. 2024).  $N_{\text{HI}}/(f/T_{\text{spin}})$  gives the normalised absorption strength, followed by the spin temperature for  $N_{\text{HI}} = 3.3 \times 10^{22} \text{cm}^{-2}$ .

Source	$z$	$N_{\text{HI}}/(f/T_{\text{spin}})$ ( $\text{cm}^{-2} \text{K}^{-1}$ )	$T_{\text{spin}}$ (K)
WISEA J022928.93+004429.5	1.217	$1.35 \times 10^{20}$	$\lesssim 240$
RCS 01020400291	1.163	$1.45 \times 10^{20}$	$\lesssim 230$
MRC 0531-237	0.851	$2.63 \times 10^{20}$	$\lesssim 130$
SDSS J090331.57+010847.5	0.522	$2.14 \times 10^{20}$	$\lesssim 150$
WISEA J145239.38+062738.2	0.267	$1.32 \times 10^{20}$	$\lesssim 250$

selection of objects faint in the  $B$ -band at  $z \gtrsim 3$ , which were sufficiently bright to yield an optical redshift, selected only objects which were very UV luminous in the source rest-frame.

Of the three high redshift exceptions where HI has been detected, two<sup>b</sup> have relatively low photo-ionisation rates ( $Q_{\text{HI}} \lesssim 10^{54} \text{s}^{-1}$ , see Fig. 3). For these, the redshifts were obtained from spectroscopy of the near-infrared band (Lawrence, Cohen, & Oke 1995; Lilly, Longair, & Allington-Smith 1985, respectively), thus remaining clear of the rest-frame  $\lambda \leq 1216 \text{Å}$  range, where the hydrogen becomes excited and subsequently ionised. For the other  $z \gtrsim 3$  detection (8C 0604+728 at  $z = 3.530$ , Aditya et al. 2021), the redshift was obtained by deep optical observations towards a previously identified radio source (Jorgenson et al. 2006).<sup>i</sup>

### 3.3. HI 21-cm absorption at the highest ionisation rate

From our fitting, the highest ionising photon rate at which HI absorption has been detected (Aditya & Kanekar 2018a) occurs at  $Q_{\text{HI}} = 2.9 \times 10^{56} \text{s}^{-1}$ , in PKS 1200+045 at  $z = 1.226$  (Fig. 6). This is the same as the theoretical  $Q_{\text{HI}}$  required to ionise all of the gas in the Milky Way (Curran & Whiting 2012). However, this was based on the simple exponential distribution, which we have shown to overestimate the column density (Section 3.2).

To obtain a revised value of the critical ionising photon rate, we again start with the ionisation and recombination of the gas in equilibrium (Osterbrock 1989),

$$Q_{\text{HI}} = 4\pi \int_0^{r_{\text{str}}} n_p n_e \alpha_A r^2 dr \quad (10)$$

where  $n_p$  and  $n_e$  are the proton and electron densities, respectively, and  $\alpha_A$  the radiative recombination rate coefficient of hydrogen. We use here the canonical  $T = 10\,000 \text{K}$  for ionised gas, giving  $\alpha_A = 4.19 \times 10^{-13} \text{cm}^3 \text{s}^{-1}$  (Osterbrock & Ferland 2006).<sup>j</sup> For a neutral plasma,  $n_p = n_e = n$ , and complete ionisation of the gas ( $r_{\text{str}} = \infty$ ), the compound model gives

$$Q_{\text{HI}} = 4\pi \alpha_A n_0^2 \left( \left[ \frac{r^3}{3} \right]_0^{r_0} + \int_{r_0}^{\infty} e^{-2(r-r_0)/R} r^2 dr \right) \quad (11)$$

$$= \pi \alpha_A n_0^2 \left( \frac{4r_0^3}{3} + R [2r_0^2 + 2Rr_0 + R^2] \right), \quad (12)$$

<sup>b</sup>J0414+0534 at  $z = 2.636$ , (Moore, Carilli, & Menten 1999) and 0902+34 at  $z = 3.398$  (Uson, Bagri, & Cornwell 1991).

<sup>i</sup>Aditya et al. (2021) claim  $Q_{\text{HI}} \approx 2 - 5 \times 10^{56} \text{s}^{-1}$  for this source, although our photometry search could only find a single value with  $\log_{10} \nu \geq 15.1$  in the rest-frame. Nevertheless, this ionising photon rate remains in the ballpark of the critical value.

<sup>j</sup><http://amdpp.phys.strath.ac.uk/tamoc/DATA/RR/>.

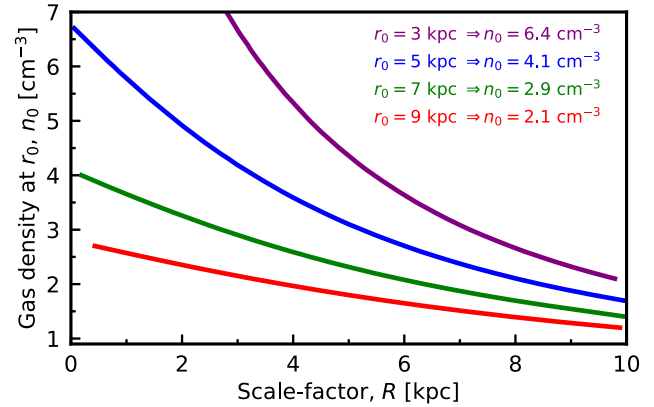


**Figure 9.** The gas density at  $r_0$  versus the scale-length required for all of the gas to be ionised by  $Q_{\text{HI}} = 2.9 \times 10^{56} \text{s}^{-1}$ .  $r_0 = 7 \text{kpc}$  for the Milky Way (Kalberla & Kerp 2009) and the key shows the value of  $n_0$  required for the Milky Way's  $R = 3.15 \text{kpc}$ .

which for  $r_0 = 0$  becomes the simple exponential model at large radii,  $Q_{\text{HI}} = \pi \alpha_A n_0^2 R^3$  (Curran & Whiting 2012). An important feature of this is that the radius of the Strömgen sphere becomes infinite for a finite photo-ionisation rate, giving the abrupt cut-off in HI detections seen in the observations.

From Equation (12), the ionising photon rate to ionise all of the gas in the Milky Way is revised to  $Q_{\text{HI}} = 7.6 \times 10^{55} \text{s}^{-1}$ , which is a factor of four lower than for the simple exponential model. Of course all of gas need not be ionised to be rendered below the detection limits of current radio telescopes, although the apparently abrupt cut-off in the detection of HI at  $Q_{\text{HI}} \lesssim 10^{56} \text{s}^{-1}$  has persisted in all of the published searches since Curran et al. (2008b) [see Section 1].

In Fig. 9 we show the ‘tweaking’ required to the Galactic gas distribution to increase the critical value to  $Q_{\text{HI}} = 2.9 \times 10^{56} \text{s}^{-1}$ . For example, for the same values of  $R$  and  $r_0$  as the Milky Way, the central density would have to be doubled to  $n_0 = 2.9 \text{cm}^{-3}$ . Conversely, keeping  $n_0 = 1.45 \text{cm}^{-3}$  gives the values of  $r_0$  and  $R$  listed in Table 2.

From these parameters we estimate column densities which are approximately equal to the maximum expected (Section 3.2) and use these to estimate possible  $T_{\text{spin}}/f$  values, all of which are very high. While low covering factors ( $f \ll 1$ ) could contribute to these, high spin temperatures would be expected from the strong UV continuum (Field 1959; Bahcall & Ekers 1969).<sup>k</sup>

In the table we also show the total gas masses, obtained from  $M_{\text{gas}} = \int_0^{\infty} \rho dV$ , where the volume of the disc gives  $dV = 2\pi t r dr$ , with  $t$  being its thickness. In the Galaxy the thickness is related to the galactocentric radius via the flare factor,  $F = r/t \approx 20$  (Kalberla & Kerp 2009), giving for the compound model:

$$M_{\text{gas}} = \frac{2\pi}{F} n_0 m_p \left( \left[ \frac{r^3}{3} \right]_0^{r_0} + \int_{r_0}^{\infty} e^{-(r-r_0)/R} r^2 dr \right), \quad (13)$$

which gives

$$M_{\text{gas}} = \frac{2\pi}{F} n_0 m_p \left( \frac{r_0^3}{3} + R [r_0^2 + 2Rr_0 + 2R^2] \right). \quad (14)$$

<sup>k</sup>With an absorption strength of  $N_{\text{HI}} = 7.8 \times 10^{18}$  ( $T_{\text{spin}}/f$ )  $\text{cm}^{-2}$ , this model yields  $T_{\text{spin}}/f \approx 6\,000 \text{K}$  for 8C 0604+728 at  $z = 3.530$  (see previous section).

**Table 2.** The required scale-length for various values of  $r_0$  to yield complete ionisation for  $Q_{\text{HI}} = 2.9 \times 10^{56} \text{ s}^{-1}$  and  $n_0 = 1.45 \text{ cm}^{-3}$ . The column densities are calculated from Equation (9) and  $T_{\text{spin}}/f$  from the measured  $N_{\text{HI}} = 4.6 \times 10^{18} (T_{\text{spin}}/f) \text{ cm}^{-2}$  (Aditya & Kanekar 2018a). The gas masses are calculated from Equation (14) using the Galactic flare factor (Kalberla & Kerp 2009).

$r_0$ (kpc)	$R$ (kpc)	$N_{\text{HI}} (\text{cm}^{-2})$	$T_{\text{spin}}/f$ (K)	$M_{\text{gas}} (M_{\odot})$
$< 7$	$> 10$	$\lesssim 4 \times 10^{22}$	$\lesssim 9\,000$	$\gtrsim 4 \times 10^{10}$
7.0	9.3	$5.3 \times 10^{22}$	12 000	$3.5 \times 10^{10}$
8.0	8.2	$5.1 \times 10^{22}$	11 000	$3.3 \times 10^{10}$
9.0	7.1	$5.1 \times 10^{22}$	11 000	$3.1 \times 10^{10}$
10.0	5.9	$5.1 \times 10^{22}$	11 000	$2.8 \times 10^{10}$
11.0	4.5	$5.3 \times 10^{22}$	12 000	$2.4 \times 10^{10}$
12.0	3.0	$5.6 \times 10^{22}$	12 000	$1.9 \times 10^{10}$
$\gtrsim 13$	$\lesssim 1$	$\gtrsim 6 \times 10^{22}$	$\gtrsim 13\,000$	$\lesssim 1 \times 10^{10}$

The H I masses derived from Equation (14) (Table 2) are close to the maximum observed in 1 000 low redshift galaxies ( $M_{\text{gas}} = 4 \times 10^{10} M_{\odot}$ , Koribalski et al. 2004), indicating that  $Q_{\text{HI}} \sim 3 \times 10^{56} \text{ s}^{-1}$  is approaching the critical value above which all of the gas in most galaxies will be ionised.

#### 4. Conclusions

From the complete photometry of each of the 924  $z \geq 0.1$  radio sources searched for in H I 21-cm absorption, we have collated the ionising photon rates and radio luminosities, finding:

- The highest ionising photon rate at which H I has been detected remains  $Q_{\text{HI}} \approx 3 \times 10^{56} \text{ s}^{-1}$ , which is close to the value required to ionise all of the neutral gas in a large spiral galaxy, thus confirming that the dearth of H I detections at high redshift is due to the bias towards sources which are most UV luminous in the rest-frame.
- Both the ionising photon rate and radio luminosity are anti-correlated with the strength of the H I absorption, although the  $Q_{\text{HI}}$  correlation is the strongest. Also, unlike the ionising photon rate, there is no critical radio luminosity above which H I is not detected. That is, ionisation of the gas, rather than excitation to the upper hyper-fine level, appears to be the dominant mechanism for the dearth of H I absorption at high redshift.
- Any evolution in the source morphologies or gas properties cannot explain the decrease in detection rate with redshift as holistically as the ionisation hypothesis.
- Detections rates are higher in galaxies than in quasars, which we attribute to the quasars generally being more luminous in the UV. It is possible that orientation effects play a role, although being a type 1 object does not necessarily exclude the detection of H I absorption. This suggests that the absorption primarily occurs in the large-scale galactic disc, as opposed to the pc-scale obscuring torus.

From the total neutral hydrogen column density of the Milky Way (Kalberla & Kerp 2009), and that expected from theory, we find:

- The strengths of the five recently detected H I absorbers with  $N_{\text{HI}} \gtrsim 10^{20} (T_{\text{spin}}/f) \text{ cm}^{-2}$  (Chowdhury et al. 2020; Murthy et al. 2021; Su et al. 2022; Aditya et al. 2024), imply spin temperatures of  $T_{\text{spin}}/f \lesssim 300 \text{ K}$ , which are typical of the Milky Way (Strasser & Taylor 2004; Dickey et al. 2009). Sufficient UV photometry to obtain the ionising photon rate is only available for one of these, but with  $Q_{\text{HI}} = 2.4 \times 10^{53} \text{ s}^{-1}$  this is three orders of magnitude below the critical value above which we expect all of the gas to be ionised.
- Conversely, for the detection of H I at the highest ionising photon rate ( $Q_{\text{HI}} = 2.9 \times 10^{56} \text{ s}^{-1}$ ), we estimate  $T_{\text{spin}}/f \sim 12\,000 \text{ K}$  which is consistent with a high ionisation fraction.
- At this ionising photon rate we calculate a gas mass of  $M_{\text{gas}} \approx 3 \times 10^{10} M_{\odot}$ , which is close to the maximum value observed in a survey of a 1 000 low redshift galaxies (Koribalski et al. 2004).

The model is, of course, an idealisation, based upon the gas distribution of the Milky Way and taking no account of shielding by dust<sup>1</sup> or regions of denser gas (e.g. molecular clouds). However, it is remarkable that it comes close to yielding the maximum ionising photon rate at which H I has been detected for a gas distribution so similar to that of a large spiral galaxy. Thus, both the extensive observational results and the model suggest that ionisation by  $\lambda \leq 912 \text{ \AA}$  photons is the dominant reason for the non-detection of cold, neutral gas within the host galaxies of high redshift radio sources.

**Acknowledgements.** I would like to thank the anonymous referee for their prompt and supportive feedback. This research has made use of the NASA/IPAC Extragalactic Database (NED) which is operated by the Jet Propulsion Laboratory, California Institute of Technology, under contract with the National Aeronautics and Space Administration and NASA's Astrophysics Data System Bibliographic Service. This research has also made use of NASA's Astrophysics Data System Bibliographic Service and ASURV Rev 1.2 (Lavalley, Isobe, & Feigelson 1992), which implements the methods presented in Isobe et al. (1986).

**Data availability.** Data available on request.

#### References

- Aditya, J. N. H. S., Jorgenson, R., Joshi, V., Singh, V., An, T., & Chandola, Y. 2021, MNRAS, 500, 998
- Aditya, J. N. H. S., & Kanekar, N. 2018a, MNRAS, 473, 59
- Aditya, J. N. H. S., & Kanekar, N. 2018b, MNRAS, 481, 1578
- Aditya, J. N. H. S., Kanekar, N., & Kurapati, S. 2016, MNRAS, 455, 4000
- Aditya, J. N. H. S., et al. 2024, MNRAS, 527, 8511
- Allison, J. R., et al. 2012, MNRAS, 423, 2601
- Antonucci, R. R. J. 1993, ARA&A, 31, 473
- Antonucci, R. R. J., & Miller, J. S. 1985, ApJ, 297, 621
- Bahcall, J. N., & Ekers, R. D. 1969, ApJ, 157, 1055
- Chowdhury, A., Kanekar, N., & Chengalur, J. N. 2020, ApJ, 900, L30
- Curran, S. J. 2012, ApJ, 748, L18
- Curran, S. J. 2019, MNRAS, 484, 3911
- Curran, S. J. 2020, A&A, 635, A166

<sup>1</sup>Which may be countered somewhat by the UV photometry being uncorrected for dust, rendering the values as relative rather than absolute.

- Curran, S. J., Allison, J. R., Glowacki, M., Whiting, M. T., & Sadler, E. M. 2013c, *MNRAS*, 431, 3408
- Curran, S. J., Allison, J. R., Whiting, M. T., Sadler, E. M., Combes, F., Pracy, M. B., Bignell, C., & Athreya, R. 2016, *MNRAS*, 457, 3666
- Curran, S. J., Hunstead, R. W., Johnston, H. M., Whiting, M. T., Sadler, E. M., Allison, J. R., & Bignell, C. 2017b, *MNRAS*, 470, 4600
- Curran, S. J., Hunstead, R. W., Johnston, H. M., Whiting, M. T., Sadler, E. M., Allison, J. R., & Athreya, R. 2019, *MNRAS*, 484, 1182
- Curran, S. J., Koribalski, B. S., & Bains, I. 2008a, *MNRAS*, 389, 63
- Curran, S. J., & Whiting, M. T. 2010, *ApJ*, 712, 303
- Curran, S. J., & Whiting, M. T. 2012, *ApJ*, 759, 117
- Curran, S. J., *et al.* 2011, *MNRAS*, 413, 1165
- Curran, S. J., Whiting, M. T., Allison, J. R., Tanna, A., Sadler, E. M., & Athreya, R. 2017a, *MNRAS*, 467, 4514
- Curran, S. J., Whiting, M. T., Sadler, E. M., & Bignell, C. 2013a, *MNRAS*, 428, 2053
- Curran, S. J., Whiting, M. T., Tanna, A., Sadler, E. M., Pracy, M. B., & Athreya, R. 2013b, *MNRAS*, 429, 3402
- Curran, S. J., Whiting, M. T., Wiklind, T., Webb, J. K., Murphy, M. T., & Purcell, C. R. 2008b, *MNRAS*, 391, 765
- Deka, P. P., *et al.* 2024, *A&A*
- Dickey, J. M., Strasser, S., Gaensler, B. M., Haverkorn, M., Kavars, D., McClure-Griffiths, N. M., Stil, J., & Taylor, A. R. 2009, *ApJ*, 693, 1250
- Field, G. B. 1959, *ApJ*, 129, 536
- Geréb, K., Maccagni, F. M., Morganti, R., & Oosterloo, T. A. 2015, *A&A*, 575, 44
- Grasha, K., Darling, J. K., Bolatto, A. D., Leroy, A., & Stocke, J. 2019, *ApJS*, 245, 3
- Heithausen, A., Brüns, C., Kerp, J., & Weiss, A. 2001, in Vol. 460, *The Promise of the Herschel Space Observatory*, G. L. Pilbratt, J. Cernicharo, A. M. Heras, T. Prusti, & R. Harris, 431
- Isobe, T., Feigelson, E., & Nelson, P. 1986, *ApJ*, 306, 490
- Jorgenson, R. A., Wolfe, A. M., Prochaska, J. X., Lu, L., Howk, J. C., Cooke, J., Gawiser, E., & Gelino, D. M. 2006, *ApJ*, 646, 730
- Kalberla, P. M. W., & Kerp, J. 2009, *ARA&A*, 47, 27
- Kaplan, E. L., & Meier, P. 1958, *JASA*, 53, 457
- Koribalski, B. S., *et al.* 2004, *AJ*, 128, 16
- Lavalley, M. P., Isobe, T., & Feigelson, E. D. 1992, in *BAAS*, 839
- Lawrence, C. R., Cohen, J. G., & Oke, J. B. 1995, *AJ*, 110, 2583
- Lilly, S. J., Longair, M. S., & Allington-Smith, J. R. 1985, *MNRAS*, 215, 37
- Maccagni, F. M., Morganti, R., Oosterloo, T. A., Geréb, K., & Maddox, N. 2017, *A&A*, 604, A43
- Mahony, E. K., *et al.* 2022, *MNRAS*, 509, 1690
- Miller, J. S., & Goodrich, B. F. 1987, *BAAS*, 19, 695
- Moore, C. B., Carilli, C. L., & Menten, K. M. 1999, *ApJ*, 510, L87
- Morgan, W. W., Whitford, A. E., & Code, A. D. 1953, *ApJ*, 118, 318
- Murthy, S., Morganti, R., Kanekar, N., & Oosterloo, T. 2022, *A&A*, 659, A185
- Murthy, S., Morganti, R., Oosterloo, T., & Maccagni, F. M. 2021, *A&A*, 654, A94
- Osterbrock, D. E., 1978, *PNAS*, 75, 540
- Osterbrock, D. E. 1989, *Astrophysics of Gaseous Nebulae and Active Galactic Nuclei* (Mill Valley, California: University Science Books)
- Osterbrock, D. E., & Ferland, G. J. 2006, *Astrophysics of Gaseous Nebulae and Active Galactic Nuclei* (Sausalito, California: University Science Books)
- Pihlström, Y. M., Conway, J. E., & Vermeulen, R. C. 2003, *A&A*, 404, 871
- Planck Collaboration, *et al.* 2020, *A&A*, 641, A6
- Purcell, E. M., & Field, G. B. 1956, *ApJ*, 124, 542
- Reach, W. T., Koo, B.-C., & Heiles, C. 1994, *ApJ*, 429, 672
- Schaye, J. 2001, *ApJ*, 562, L95
- Skrutskie, M. F., *et al.* 2006, *AJ*, 131, 1163
- Strasser, S., & Taylor, A. R. 2004, *ApJ*, 603, 560
- Su, R., *et al.* 2022, *MNRAS*, 516, 2947
- Su, R., *et al.* 2023, *ApJ*, 956, L28
- Uson, J. M., Bagri, D. S., & Cornwell, T. J. 1991, *PhRvL*, 67, 3328
- Vermeulen, R. C., *et al.* 2003, *A&A*, 404, 861
- Wright, E. L., *et al.* 2010, *AJ*, 140, 1868